Lawrence Berkeley National Laboratory
Recent Work

Title

RAMAN CHARACTERIZATION OF HIGH TEMPERATURE MATERIALS USING AN IMAGING DECTECTOR

Permalink

https://escholarship.org/uc/item/6rv9k1qb

Authors

Rosenblatt, G.M.
Veirs, D.K.

Publication Date

1989-03-01

Lawrence Berkeley Laboratory
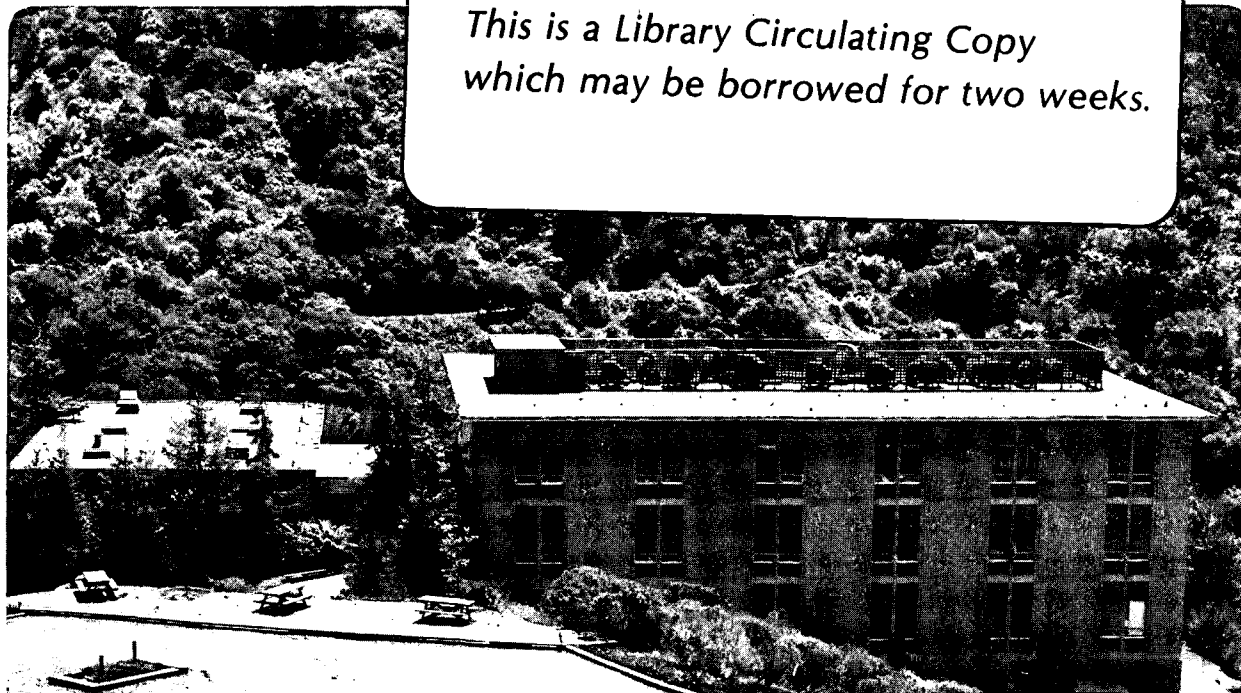
UNIVERSITY OF CALIFORNIA

Materials & Chemical Sciences Division

Raman Characterization of High Temperature Materials Using an Imaging Detector

G.M. Rosenblatt and D.K. Veirs

March 1989

DISCLAIMER

Raman Characterization of High Temperature Materials Using an Imaging Detector

Gerd M. Rosenblatt and D. Kirk Veirs
Lawrence Berkeley Laboratory
Materials and Chemical Sciences Division
1 Cyclotron Road
Berkeley, CA 94720

(March 15, 1989)

Abstract

The characterization of materials by Raman spectroscopy has been advanced by recent technological developments in light detectors. Imaging photomultiplier-tube detectors are now available that impart position information in two dimensions while retaining photon-counting sensitivity, effectively greatly reducing noise. The combination of sensitivity and reduced noise allows smaller amounts of material to be analyzed. The ability to observe small amounts of material when coupled with position information makes possible Raman characterization in which many spatial elements are analyzed simultaneously. Raman spectroscopy making use of these capabilities has been used, for instance, to analyze the phases present in carbon films and fibers and to map phase-transformed zones accompanying crack propagation in toughened zirconia ceramics.

Index Entries

Raman spectroscopy, imaging, carbon, zirconia, toughened

INTRODUCTION

Understanding the chemistry and molecular architecture which underlies the physical properties of many materials requires chemical characterization of the material; i.e., characterization of the chemical composition, bonding and thermodynamic phase. With films, fibers, and many high-tech materials, sample volumes may be small and a sensitive chemical characterization technique is required. For instance, thin films of pure carbon exhibit a wide variety of electrical, mechanical and physical properties that depend upon the microscopic morphology which may encompass diamond, graphite and a wide range of amorphous or intermediate structures. Although the two common crystalline forms of pure carbon, graphite and diamond, are easily distinguished in bulk quantities by X-ray diffraction, thin films of pure carbon are extremely difficult to characterize using X-ray diffraction because of small signals and, in the case of amorphous films, the absence of long-range order.

In some cases macroscopic physical properties depend upon the chemical nature of the material changing across small distances. In these cases spatially-resolved chemical characterization is needed. For instance, ceramics which are strong but also unusually resistant to brittle fracture are produced by the controlled use of martensitic transformations, i.e., at least partly irreversible transformations between two solid phases having the same chemical composition.[1] The anticipated increase in toughness has been demonstrated for cubic zirconia ceramics containing precipitates of tetragonal and monoclinic ZrO_2. When a crack propagates in this material, the metastable tetragonal zirconia particles martensitically transform to the monoclinic phase in the high stress fields associated with the crack tip, forming a transformed zone surrounding the crack and crack tip. This transformation is thought to be a significant factor in the toughening of these materials. Theoretical approaches to understanding the fracture resistance of these materials indicate that toughening depends upon the zone width, the shape of the transformed zone around the crack tip, the extent of transformation within the zone, and the degree of irreversibility of the martensitic transformation. Understanding and optimizing the fracture resistance of such materials requires determining the phase composition in the transformed zone surrounding the crack with a spatial resolution of better than 50 μm.

For both of these examples the distinguishing feature between the various forms of the materials is the difference in bonding (bond lengths, bond angles, and bond strengths) and not the chemical composition. This difference alters the fundamental atom-atom vibrations in the microcrystallites composing the material and can be detected using vibrational spectroscopy. Vibrational Raman spectroscopy is an optical technique in which scattered light is shifted in frequency by an energy equal to the energy difference between vibrational energy levels in the scattering material. The vibrational spectrum of a material is obtained by measuring the shift in energy of light scattered from a material illuminated with a monochromatic source. All materials have Raman-active vibrations with the one exception of a purely cubic phase.

The difficulty with Raman spectroscopy is that only a very small fraction of the incident light is Raman scattered. This means that it is not always easy to achieve reasonable signal:noise levels because of interference from other optical processes such as fluorescence or because of small signals in the case of small volumes. Recent advances in optical detectors have produced two-dimensional "imaging" detectors that have low noise and single-photon sensitivity. Such detectors, when carefully coupled with other recent advances in instrumentation, make it possible to apply Raman spectroscopy to materials problems which were formerly unaccessible to study because of the small sample volumes involved or the spatial resolution required.

In this paper we summarize some of the characteristics of a Raman apparatus built in our laboratory that utilizes an imaging photomultiplier tube for materials characterization. The salient capabilities are low noise, high sensitivity, and the capability to obtain one-dimensional profiles of chemical phase from a single illumination without moving the sample or scanning the spectrometer. Moving the sample allows subsequent profiles to be combined to produce a two-dimensional map of chemical phase. The characteristics and capabilities of the approach are illustrated by summaries of recent experiments in our laboratory on carbon films and fibers and on the phase-transformed zone surrounding cracks in phase- stabilized zirconia.

EXPERIMENTAL METHOD

The major problem with the use of Raman scattering for the characterization of materials is that it is a weak phenomenon; the Raman cross-section for most materials is 10^{-31} cm^2 sr^{-1}. This means that a 100 mW laser beam that illuminates a typical solid sample with 2×10^{17} photons s^{-1} produces about 10^{10} Raman scattered photons s^{-1} sr^{-1}; these must be collected and spectrally dispersed to yield useful information. Even with bright light sources (lasers) and sensitive detectors (photon-counting photomultiplier tubes (PMTs)), long integration times are necessary to obtain good signal-to-noise ratios (S/N). Advances in multi-channel detectors, in particular the advent of the intensified photodiode array (IPDA), have increased the sensitivity of Raman spectroscopy. Using an IPDA coupled to a microscope, commercial Raman microprobe instruments have demonstrated utility in investigating a number of materials problems which require a single point analysis of a small volume.[2] At the present time, a new generation of sensitive detectors is available which produce data resolved in two position dimensions (X and Y) in contrast to the one-dimensional resolution (X) of the IPDA. These new detectors, which include the imaging PMT and charge coupled device (CCD), also have less background and hence lower noise characteristics than the IPDA. These sensitive and low noise detectors can be used to extend the capabilities of Raman spectroscopy to investigate small amounts of material and to obtain multiplexed, spatially resolved, Raman spectra with a few microns spatial resolution.

The results presented here were obtained with a Raman spectroscopy apparatus incorporating an imaging PMT detector. This detector has several intrinsic features which allow a Raman spectrum to be obtained with both high sensitivity and multiplexed spatial resolution. First, the 25 mm diameter active region is partitioned into a 1024 x 1024 x $\frac{\pi}{4}$ data array (the photoresponsive region is a disk that inscribes a 1024 x 1024 square). The detector is oriented so that one dimension (X) corresponds to the wavelength dispersion of the spectrometer and the second dimension (Y) corresponds to distance along the sample. Second, the detector dark count which totals 30 counts per second (cps) at -30 °C is spread out over the 8×10^5 active pixels yielding a dark count rate per pixel of just 4×10^{-5} cps. Thus, detector dark count is virtually eliminated as a noise source.

The Raman system has been described previously[3] and only the main features and major changes will be emphasized. The apparatus consists of a cw Ar$^+$ laser usually operated at 488.0 nm, focusing and collection optics, single spectrometer, imaging PMT detector, and microcomputer data acquisition. The Raman shifted light is isolated by a six-cavity interference filter which rejects the unshifted Rayleigh line by about six orders of magnitude while passing the region of interest with about 70% transmission. The interference filter used for Rayleigh- scattering rejection adds an additional (rapidly varying) wavelength response to the (normally slowly varying) response of the spectrometer and detector. If accurate determinations of intensity ratios using an apparatus of the type described here are needed, the instrument response should be measured and used to correct the raw data.

Data are collected in two distinct modes depending upon whether or not a spatially-resolved profile is desired. When spatial resolution is not being sought the laser is focused to a spot of about 50 μm diameter on the sample using a single lens. The scattered light is collected and focused onto the entrance slit of the spectrometer. The vertical dimension data are summed over a defined active region (typically ca. 100 rows) while wavelength dispersed information is retained. In this case, the detector dark count per wavelength channel is given by the number of rows which are active ($\sim$100) times the dark count per pixel, approximately 3 x 10^{-3} cps per wavelength channel. The S/N of solid samples is always dominated by noise due to background signals from the sample. Many materials fluoresce strongly and special techniques not practical in our apparatus such as Fourier Transform Raman are needed to obtain their Raman spectra.[4]

When spatial resolution is required the laser beam is expanded and then focused on the sample using a cylindrical lens. This produces a slit like illumination of 30 μm x 2.5 mm which is imaged onto the entrance slit of the spectrometer. The cylindrical lens is rotated to align the image with the entrance slit. Each row in the detector array, corresponding to one spatial element along the illumination line at the sample, contains a unique Raman spectrum which can be analyzed to determine the chemical composition within that spatial element of the sample. Computer memory restrictions in our apparatus dictate that the data be acquired in a 256k position array. When desired this can be accumulated as a 256 wide x 1024 high matrix where the spatial dimension retains the high resolution. Because

approximately 800 rows of the detector data array are illuminated, this configuration simultaneously yields 800 Raman spectra from 800 consecutive spatial elements along the sample; from these a 800-position chemical profile can be derived. The integration times are typically less than 400 seconds with a maximum detected total count rate of about 10^4 cps which yields 5×10^3 counts over one row (256 channels wavelength channels) or an average of 20 counts per wavelength channel. The low noise characteristics of the detector allow such small signals to be obtained and analyzed; the detector contributes 0.01 total counts of background to the detected signal in one row over 400 seconds.

RESULTS AND DISCUSSION

A. CARBON THIN FILMS AND FIBERS

Graphite and diamond have quite different Raman spectra. Spear[5] notes that Raman spectroscopy is the most reliable technique for distinguishing between crystalline diamond and other various forms of carbon and suggests that a working definition for "crystalline diamond material" in vapor deposited thin films include having a Raman spectrum typical of crystalline diamond (Fig. 1). Detailed analysis of the Raman spectrum of amorphous carbon, e.g. relative peak intensities, linewidths and absolute peak positions, can be used to estimate physical and chemical properties such as the average microcrystalline domain size and the sp^2/sp^3 bonding ratio.[6]

The Raman spectrum of carbon in the 1000 cm^{-1} to 2000 cm^{-1} range has been used to study the microscopic morphology of various forms of carbon. The data are corrected for the wavelength dependent intensity response which was calibrated using a tungsten intensity calibration lamp traceable to NBS. Single crystal graphite has a single, narrow Raman peak (the G-band) at 1575 cm^{-1} and a disorder induced peak (D-band) at 1355 cm^{-1}.[7] Diamond's single, sharp Raman peak at 1332 cm^{-1} is distinct from the D-band of graphite, Fig. 1. The ratio of the integrated intensities of the D-band to the G-band has been correlated with average microcrystalline domain size, L_a, as determined by X-ray data[7] and transmission electron microscopy.[8] The observed increase in the relative intensity of the D (disorder) band relative to the G (graphite) band with decreasing microcrystallite size may reflect

7

the D-band intensity arising primarily from carbon atoms near the crystallite surface while the G-band arises from bulk-like carbon atoms in the interior volume. Linewidths of the D-band have also been correlated with L_a.[8,9] Shifts of the G-band to lower frequencies have been related to the sp^3 bonding fraction.[10,11]

Theoretical models of amorphous carbon with differing percentages of three-fold (sp^2) and fourfold (sp^3) coordinated atoms indicate that the addition of fourfold coordinated atoms produces a gradual transition in the vibrational spectra to lower frequencies rather than a mixture of distinct features typical of graphite and diamond.[10] Richter et al.[11] modeled the frequency of the G-band of graphite using force constants for both sp^2 and sp^3 bonded carbon atoms and found the shift in the frequency to lower energies to be essentially linear with increasing numbers of sp^3 bonded carbon atoms.

Thin, sputtered carbon films ~20-40 nm thick used as protective overcoats on commercial $5\frac{1}{2}$-inch computer hard disks have been investigated. The results are reported elsewhere[6] and the salient features will be summarized here. Samples from two manufacturers designated as K and L were obtained; sample K2 (450°C for 10 h) and K5 (350°C for 0.5 h) were annealed in vacuum. Raman spectra between 1000 and 2000 cm^{-1} were collected for four samples using 6.5 mW of laser power and a 1000 s integration time, Fig. 2. The spectra were fit to the sum of a linear background term and two damped oscillator line shapes. Each plot if Fig. 2 contains the corrected experimental data and three curves calculated from the fitted parameters. Two of the curves are calculated from the parameters representing the G and D bands individually and the third curve is the sum of the calculated background, D, and G bands. The standard error of the fit, defined as the RMS average of the differences between the fit and the data divided by the data, ranged from 0.027 to 0.022 for all samples. Wavelength calibration was achieved by fitting 17 Ne emission lines resulting in a 0.33 cm^{-1} standard error (less than one pixel).

From the fitting parameters one can calculate the peak position and linewidth of both the D and G bands, as well as the integrated intensity ratio, I_d/I_g. The results are shown in Table I. The observed ratios I_d/I_g are considerably larger than one. Available literature data[7] on the correlation of this ratio with domain size indicate that values close to or greater than one are always associated with graphite microcrystallite domains less than 5 nm across, but those data are limited to bulk

8

samples having $I_d/I_g \leq 1$. Ratios considerably larger than one are routinely observed in thin films.[8,11] The correlation with domain size in fine-grained films has not been measured, but measurements[8] of I_d/I_g as a function of annealing temperature suggest that for very small grains (<2 nm) I_d/I_g increases with grain size (rather than decreases) to a maximum of 2.5 for 2 nm grains, followed by a decrease in I_d/I_g (similar to that observed with coarser carbon[7]) as the grains grow further. It appears reasonable to postulate that the large I_d/I_g ratios in Table I correlate with grains smaller than 5 nm and that the grain size increases with increased annealing temperature (and also with increasing I_d/I_g) in these thin, fine- grained films. From comparison of the peak positions and widths, the microcrystallites in L3 are larger (>2 nm) than those in the K series samples (<2 nm) even though the I_d/I_g ratios for L3 and K1 are nearly equal.

For the K series carbon films the Raman data suggest that these are composed of microcrystallites of less than 2 nm with 5% sp^3 bonds. Upon annealing the sp^3 bond percentage drops essentially to 0% as the grains grow. In the L3 sample there are very few sp^3 bonds and the microcrystals still are much smaller than 5 nm, but probably larger than in the K series. Diamond spectral peaks were not observed in any sample. However, the small grains and extensive sp^3 cross-linking of the K series films correlate with these having the "diamond-like" hardness required for the intended application.

Carbon fibers used to increase the strength of composite materials have much better separated D- and G-bands. Mechanical properties of polymer fibers have been related to their crystal quality as measured by x-ray diffraction.[12] Graphite crystal quality is directly related to observables in the Raman spectra, namely the peak positions, linewidths, and intensity ratios of the 1355 (D) and 1575 (G) cm^{-1} peaks.

Fibers annealed at 2400°C, 2600°C, and 2800°C have been examined and the I_d/I_g ratio, line positions, and linewidths have been determined. The wavelength was calibrated using Ne and Ar discharge lamps and Th lines from a hollow cathode lamp to a standard error of 0.4 cm^{-1}. The data were taken with 5 mW of 488.0 nm laser light incident on a fiber with an integration time of 500 s and a slit width of 121 μm. Representative Raman spectra are shown in Fig. 3. At laser powers above 200 mW the samples (a single carbon fiber) are destroyed by the focused

laser beam.

The results are shown in Table II. The fibers have narrower D and G bands, smaller I_d/I_g intensity ratios, a D-band shifted by ca. 40 cm^{-1} to lower frequency, and an unchanged G (graphite) band position relative to the carbon films. These changes are consistent with much smaller surface:volume ratios, and larger microcrystallites, ca. 7-13 nm, than the films. Heat treatment to 2600°C shifts both the D- and G-bands to higher frequencies by about 5 cm^{-1} and decreases their linewidths by about 20% as compared to the 2400°C samples. Further heat treatment to 2800°C does not significantly change the line positions or linewidths. In contrast, heat treatment to 2800°C continues to change the intensity ratio. As discussed above, intensity ratios less than one have been correlated with the inverse of the domain size[7] yielding a linear relation. Using this relation, the microcrystallite domain size of the carbon fiber samples appears to nearly double upon increasing the temperature from 2400°C to 2800°C.

B. TRANSFORMED ZONES IN PARTIALLY STABILIZED ZIRCONIA

As mentioned in the introduction, elucidation of the toughening mechanism in high-tech phase-stabilized zirconia ceramics requires mapping the phase transformed zone surrounding cracks with a resolution of better than 50 μm. Under static loading a crack initialed in PSZ grows until a zone is formed around the crack tip where tetragonal phase has transformed martensitically into monoclinic phase. For the crack to grow further an increased static applied stress is necessary. The increased applied stress in turn produces a larger transformed zone and the crack again stops. Thus, under static loading, continously increasing applied loads are necessary for continued crack growth. However, under cyclic loading, cracks in PSZ grow without cessation.[13] Thus failure is somewhat analogous to fatigue- crack growth in metals. The mechanism of crack growth under cyclic load is not fully understood and is being investigated.

Raman spectroscopy utilizing the two-dimensional detector and techniques described above can be used to map the transformed zone.[14] A semi-automated experimental setup yields the fraction of monoclinic phase relative to the sum of the monoclinic and tetragonal phases, determined from the Raman spectrum, as a function of distance across the surface of the specimen. First, a one-dimensional

chemical profile of 800 elements is determined by analysis of the data resulting from a single 400 s slit-like illumination of a line across the sample. Second, the sample is translated a known amount perpendicular to the slit-like illumination and another one-dimensional chemical profile is determined. This process is repeated automatically and successive profiles are then combined to produce a map of the phase distribution.

The partially stabilized zirconia used for this study is composed of 50 μm grains of cubic-phase zirconia with lenticular precipitates of tetragonal and monoclinic phases with a maximum dimension of 300 nm. The tetragonal-phase precipitates, which otherwise would transform martensitically to monoclinic at room temperature, are stabilized by the addition of 9 mol% MgO. The precipitates form 35-40% by volume of the cubic grains.

A Raman spectrum typical of PSZ used in these studies is shown in Fig. 4. To calculate a phase profile, the fraction of monoclinic is computed using the integrated intensities (minus the background) of the 181 and 192 cm^{-1} peaks for the monoclinic phase and the integrated intensity (minus the background) of the 264 cm^{-1} peak for the tetragonal phase. The monoclinic and tetragonal phases are assumed to produce the same relative Raman intensities; this assumption is consistent with literature relative Raman intensities[15] and yields results that are not inconsistent (within the large, perhaps a factor of two, uncertainty in the X-ray determination) with the composition of samples determined by X-ray diffractrion. The relative Raman response of the two phases affects the scale, but not the topography of the compositional maps that are determined.

The application of spatially-resolved Raman spectroscopy to cracks grown in peak-toughened PSZ is described in detail in Ref. 14. That report describes results on a crack grown using a constant cyclic load. In subsequent work we have investigated a crack grown with a varying amplitude cyclic load, during fatigue-crack growth in a peak-toughness MgO-PSZ sample 3 mm thick.[16] The crack-growth rate exhibits sharp changes which depend upon changes in the magnitude of the load. Because the crack-growth rate depends upon the transformed zone, detailed measurements of the transformed zone are required in order to understand the behavior of the rate of crack growth and the implications for failure mechanisms under varying load conditions.

11

The specimen was cyclically loaded at a load ratio of 0.1 ($K_{min} = 0.1\ K_{max}$; where K_{min} and K_{max} are, respectively, the minimum and maximum stress intensities in a given fatigue cycle; K_{max} and K_{min} are changed together in varying-load experiments) and frequency of 50 Hz in a high-resolution, computer- controlled electro-servohydralic testing machine.[16] Crack-growth rates, dA/dN, were determined during computer controlled applied stresses over a range of $\triangle K$ ($\triangle K = K_{max}$ - K_{min}). Fig. 5 shows the applied stress and the crack-growth rate as a function of crack extension. A constant high cyclic load is first applied ($\triangle K = 9.5\ MPa\sqrt{m}$) and the crack-growth rate increases toward a steady state value. On reducing the cyclic loads somewhat (to $\triangle K = 8.5\ MPa\sqrt{m}$), a marked transient retardation in crack velocity is seen followed by a gradual increase in crack-growth rate toward a (new) steady- state velocity. A significant retardation is seen following a single tensile overload to a K_{max} of 12.3 MPa$\sqrt{m}$) (the fracture toughness of this material is $K_c = 16.0\ MPa\sqrt{m}$)).

The Raman map of the phase distribution of this sample, Fig. 6, is constructed from 65 chemical profiles taken perpendicular to the crack every 125 μm. A laser power of 150 mW and an integration time of 200 s per profile was used. Calculation of the chemical profile from each illumination takes 132 s so the total time for data collection and analysis was 6 hours ((200 s + 132 s) x 65). Further development of the data collection and computation algorithm now allow this same profile to be collected in less than 4 hours (200 s x 65). The count rate was 32000 cps and the average count per pixel was 24. The transformation zone shows considerable changes in the zone width and extent of transformation which are related to the applied stress.

The crack-growth rate can be understood qualitatively by considering the size of the transformed zone and the magnitude of the applied stress. If the transformed zone is large the rate of crack growth (under a given cyclic applied stress) will be relatively small. Conversely, if the transformed zone is small, the crack- growth rate will be relatively large. The size of the transformed zone surrounding the crack tip is dependent upon the stress that has been applied. When the applied stress is lowered from $\triangle K = 9.5\ MPa\sqrt{m}$ to $\triangle K = 8.5\ MPa\sqrt{m}$ the crack tip is surrounded by a larger transformed zone associated with the larger applied stress, and the crack- growth rate is observed to decrease sharply. As the crack grows out of this

12

large transformed zone to the smaller transformed zone associated with an applied stress of 8.5 MPa$\sqrt{m}$ the rate of crack growth is observed to increase. A large zone associated with the application of a single overload of 12.3 MPa$\sqrt{m}$ caused a rapid decrease in the crack-growth rate followed by a gradual increase in growth rate as the crack tip moved out of the large zone. Changing K_{min} without changing K_{max} does not appear to change the crack-growth rate or the size of the transformed zone.

SUMMARY

The applicability of Raman spectroscopy to materials – and to the characterization questions raised by high-technology, high-temperature and energy-related materials – has been extended by recent advances in photon detectors. The utilization of two-dimensional array detectors for Raman spectroscopy has increased the sensitivity of the technique by virtually eliminating the detector dark count as a source of noise and has resulted in the development of a new method for obtaining multiplexed, spatially- resolved Raman spectra. By using the spatial resolution of the detector to achieve spatial resolution at the sample, spectra from many spatially resolved elements at the sample can be collected and analyzed simultaneously. This simultaneous multiplexing of both wavelength and position makes use of the inherent low dark count per pixel of the detector and results in the rapid determination of a chemical composition profile. By translating the sample (in one direction) across the illuminating slit-like beam a map of the chemical composition of the sample surface can be determined. This technique for chemical mapping can be adopted to most forms of optical spectroscopy when an appropriate two-dimensional detector is used. This paper has illustrated some of these capabilities by describing results from on-going work on carbon films and fibers and on phase- stabilized zirconia ceramics.

ACKNOWLEDGMENTS

REFERENCES

1. A.G. Evans and A.H. Heuer, *J. Am. Ceram. Soc.* 63, 241 (1980).

2. L. Soto and F. Adar, *Microbeam Analysis-1984*, A.D. Romig, Jr. and J.I. Goldstein, Eds., San Francisco Press, 1984, p.121; P.V. Huong, P. Boutinaud, S. Kasaoui, and A. Leycuras, *Microbeam Analysis- 1984*, D.E. Newbury, Ed., San Francisco Press, 1988, p.167 and others in that volume.

3. D.K. Veirs, V.K.F. Chia, and G.M. Rosenblatt, *App. Opt.* 26, 3530 (1987).

4. D.B. ChasE, *J. Am. Chem. Soc.* 108, 7485 (1986); C.G. Zimba, V. Hallmark, J.D. Swalen, and J.F. Rabolt, *Appl. Spec.* 41, 761 (1987).

5. K.E. Spear, *J. Am. Ceram. Soc.* 72, 171 (1989); R. Messier, A. Badzian, T. Badzian, K.E. Spear, P. Bachmann, and R. Roy, *Thin Solid Films* 153, 1 (1987).

6. H.-c. Tsai, D.B. Bogy, M.K. Kundmann, D.K. Veirs, M.R. Hilton, and S.t. Mayer, *J. Vac. Sci. Technol. A* 6, 2307 (1988).

7. F. Tuinstra and J. L. Koenig, *J. Chem. Phys.* 53, 1126 (1970).

8. C. Beny-Bassez and J.N. Rouzaud, *Scan. Elec. Micros.* 1985, 119 (1985).

9. C.A. Johnson, J.W. Patrick and K.M. Thomas, *Fuel* 65, 1284 (1986).

10 D. Beeman, J. Silverman, R. Lynds and M.R. Anderson, *Phys. Rev. B* 30, 870 (1984); M. DiDomenico, Jr., S.H. Wemple, S.P.S. Porto and R.P. Bauman, *Phys. Rev.* 174, 522 (1968).

11. A. Richter, H.-J. Scherbe, W. Pombe, D.-W. Brzezinka, and I. Muhling, *J. Non-Crystal. Sol.* 88, 131 (1986).

12. R.J. Day, I.M. Robinson, M. Zakikhani, and R.J. Young, *Polymer* 28, 1833 (1987).

13. R.H. Dauskardt, W. Yu and R.O. Ritchie, *J. Am. Ceram. Soc.* 70, C248 (1987)

14. R.H. Dauskardt, D.K. Veirs, and R.O. Ritchie, *J. Am. Ceram. Soc.* in press.

15. D.R. Clarke and F. Adar, *Advances in Materials Characterization*, D.R. Rossington, R.A. Condrate, and R.L. Snyder, Eds., Plenum, p. 199, 1983.

16. R.H. Dauskardt, D.B. Marshall and R.O. Ritchie, *Proceedings of the Materials Research Society International Meeting*, 1988.

Table I: Positions, linewidths, and intensity ratios of the graphite and disorder induced Raman bands of carbon thin films obtained from fitting the observed data to a theoretical model. The percentage of sp^3 bonding is obtained from the shift of the G-band.

| Sample | Anneal T °C | G-BAND | | D-BAND | | I_d/I_g | % sp^3 |
		Position cm^{-1}	Linewidth cm^{-1}	Position cm^{-1}	Linewidth cm^{-1}		
K1	–	1562	176	1393	347	1.47	5
K5	350	1571	160	1391	349	1.72	2
K2	450	1575	140	1386	335	2.16	0
L3	–	1575	159	1372	300	1.54	0

Table II: Intensity ratios, domain sizes, line positions
and linewidths of Raman peaks from carbon fibers annealed
at 2400°C, 2600°C, and 2800°C.

	I_d/I_g	L_a	G-BAND		D-BAND	
			Position	Linewidth	Position	Linewidth
		nm	cm^{-1}	cm^{-1}	cm^{-1}	cm^{-1}
CF2400	0.63	6.7	1565.6	38.6	1348.8	38.2
CF2600	0.48	8.3	1572.8	32.0	1353.1	29.0
CF2800	0.28	12.5	1570.3	29.4	1354.3	31.6

FIGURE CAPTIONS

FIGURE 1: A single sharp Raman peak at 1332 cm^{-1} is a distinguishing feature of diamond thin films. The weak, broad peaks extending from 1100-1600 cm^{-1} are due to amorphous carbon which has a much larger Raman cross-section.
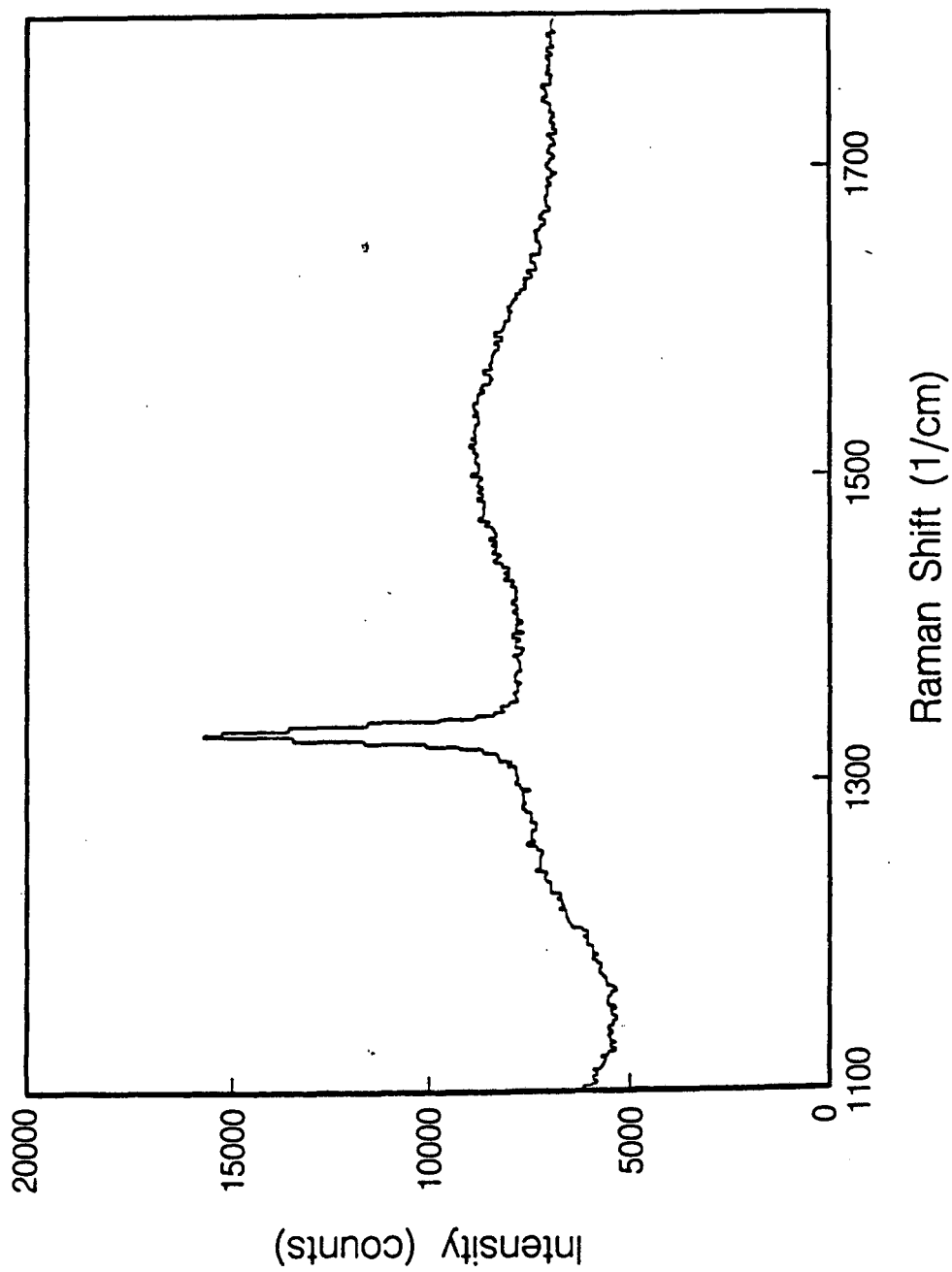
FIGURE 2: Raman spectra of the carbon overcoats on magnetic media disks from two different manufacturers. Samples K1, K5, and K2 were sectioned from the same disk and annealed at 30°C, 350°C, and 450°C respectively. The data and fit, comprised of two peaks and a background (not shown), are shown for the four samples.

FIGURE 3: The effect of annealing on single carbon fibers is seen in the Raman spectra. At higher annealing temperatures the G-line at 1575 cm^{-1} grows at the expense of the D-line at 1350 cm^{-1} and the linewidths decrease. This is an indication of graphite microcrystallite growth from 7 to 13 nm.

FIGURE 4: The tetragonal and monoclinic phases of zirconia have Raman peaks at different frequencies which can be used to determine the relative amounts of each phase. In this work the 181, 192 cm^{-1} pair is used to measure the monoclinic phase and the 264 cm^{-1} peak is used to measure the amount of tetragonal phase.

FIGURE 5: The crack growth rate and applied stress (schematic) in toughened PSZ are shown as a function of crack extension for a fatigue-crack grown under varying amplitude cyclic loads.

FIGURE 6: A map of the monoclinic phase fraction of the zirconia specimen whose applied stress and crack growth rate are shown in Fig. 5 indicates that the stress history of the material is revealed in the extent and degree of transformation of the transformed zone. Large stresses induce a larger transformed zone around the crack tip that remains after the crack tip moves forward.
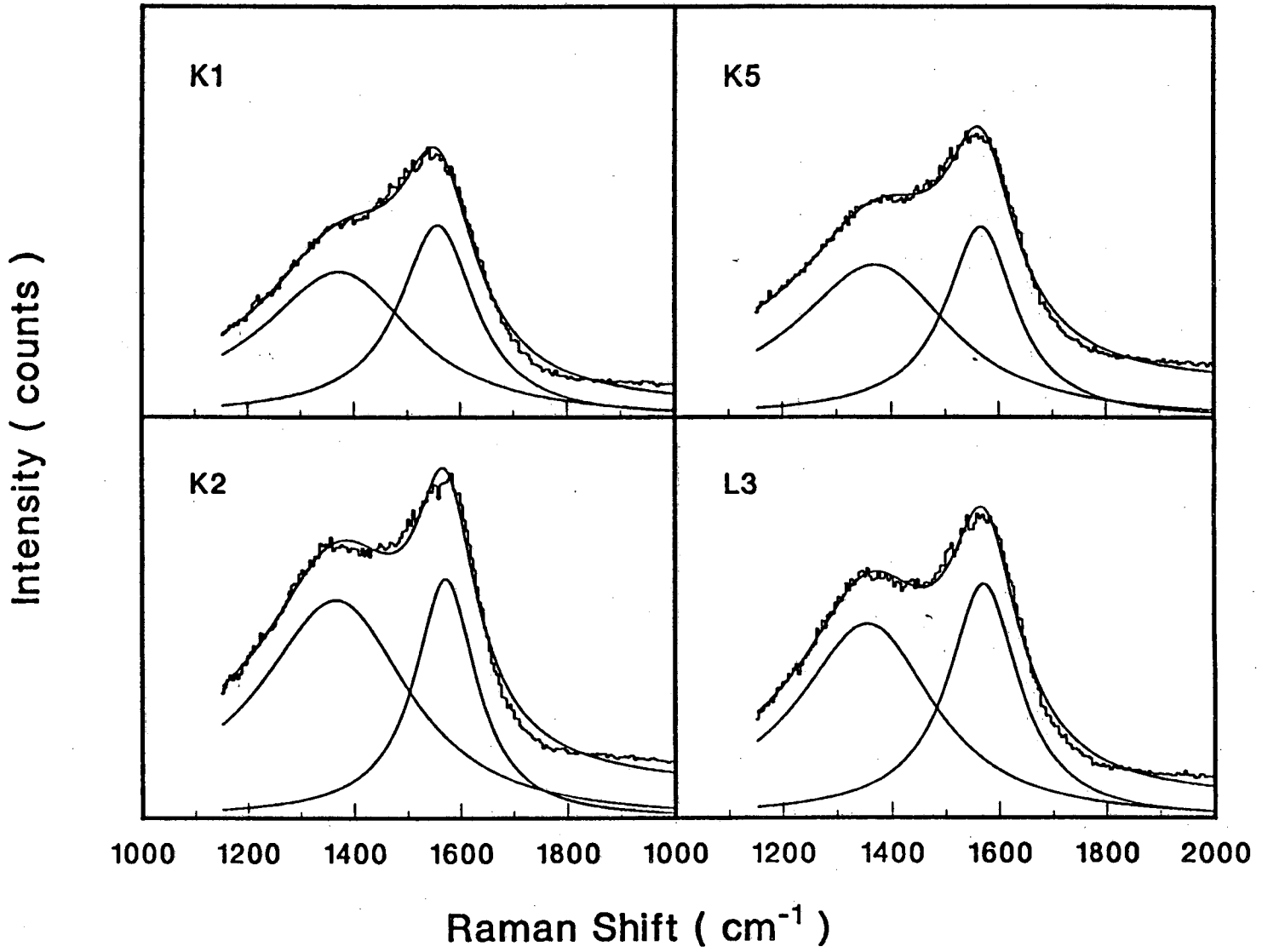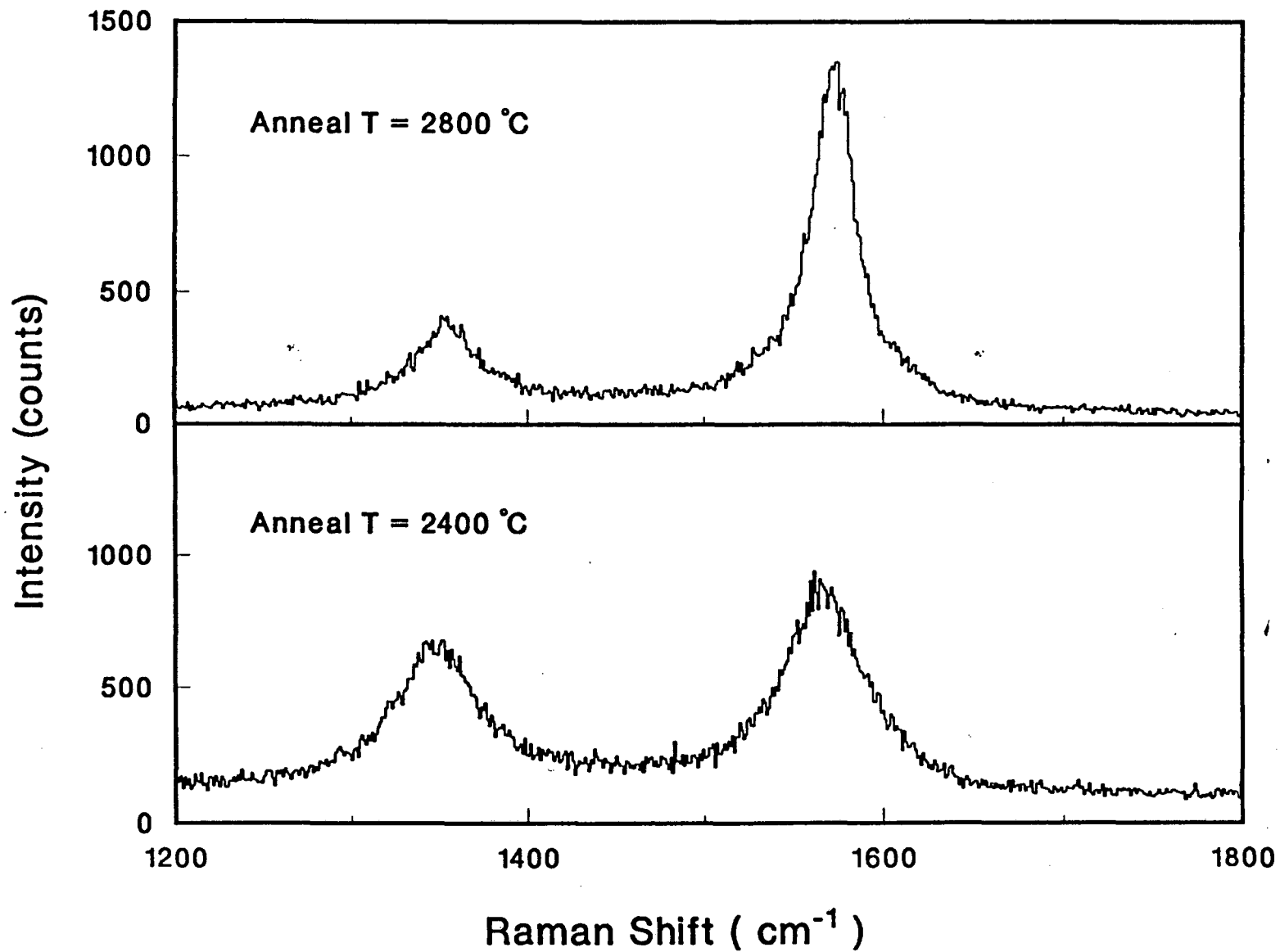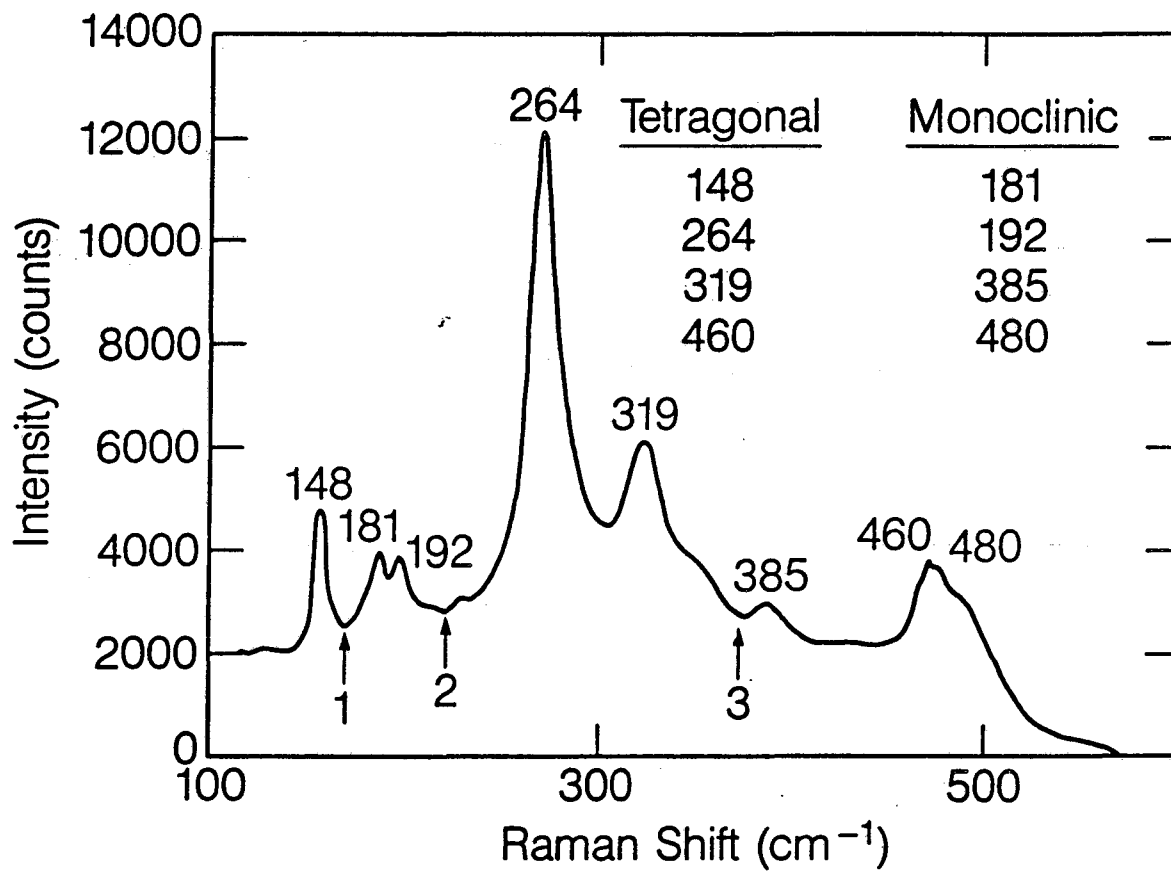
Raman Shift (1/cm)

Intensity (counts)

Fig. 1

XBL 887-8923

19

Fig. 2

XBL 893-922

Fig. 3

Intensity (counts)

Anneal T = 2800 °C
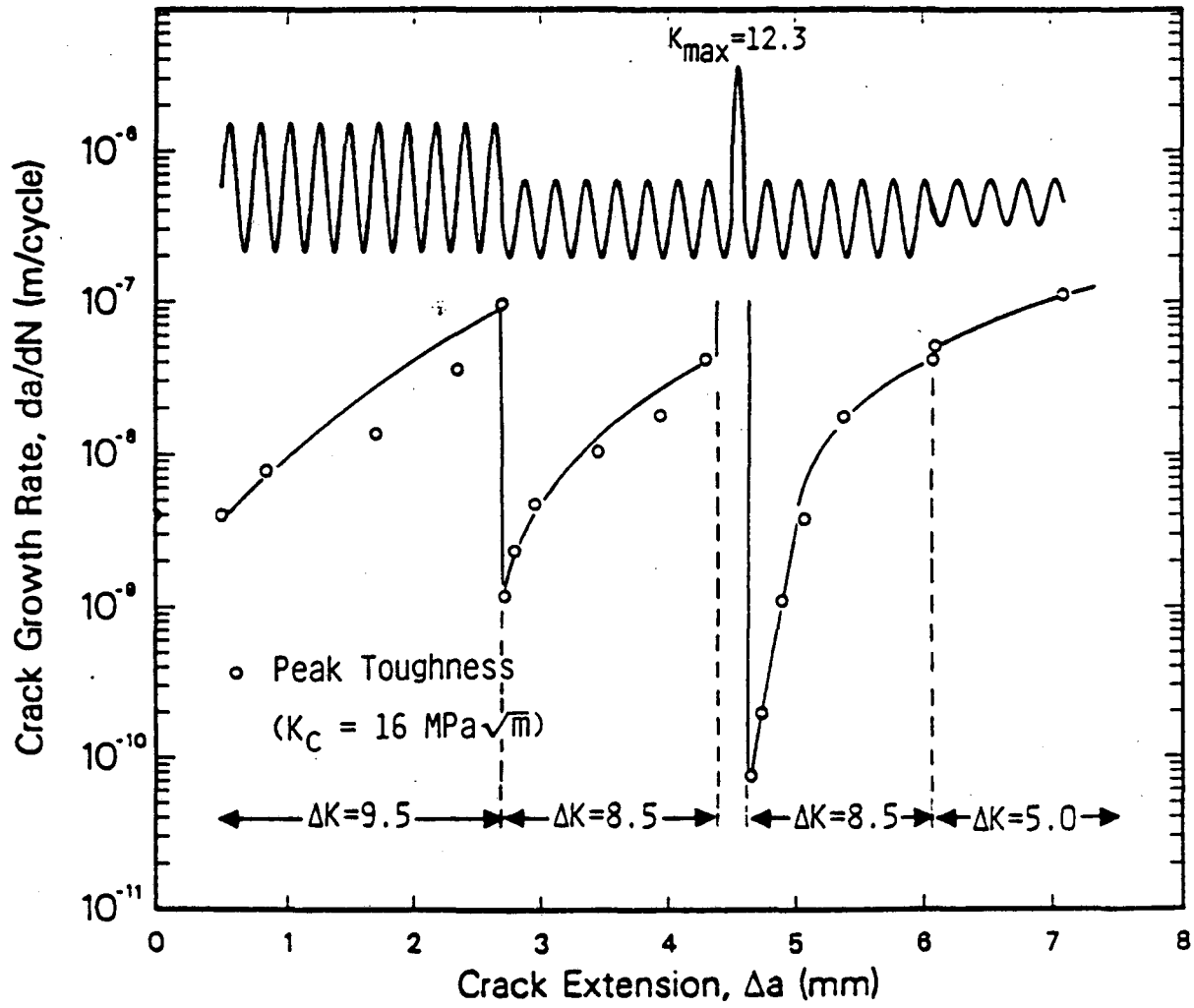
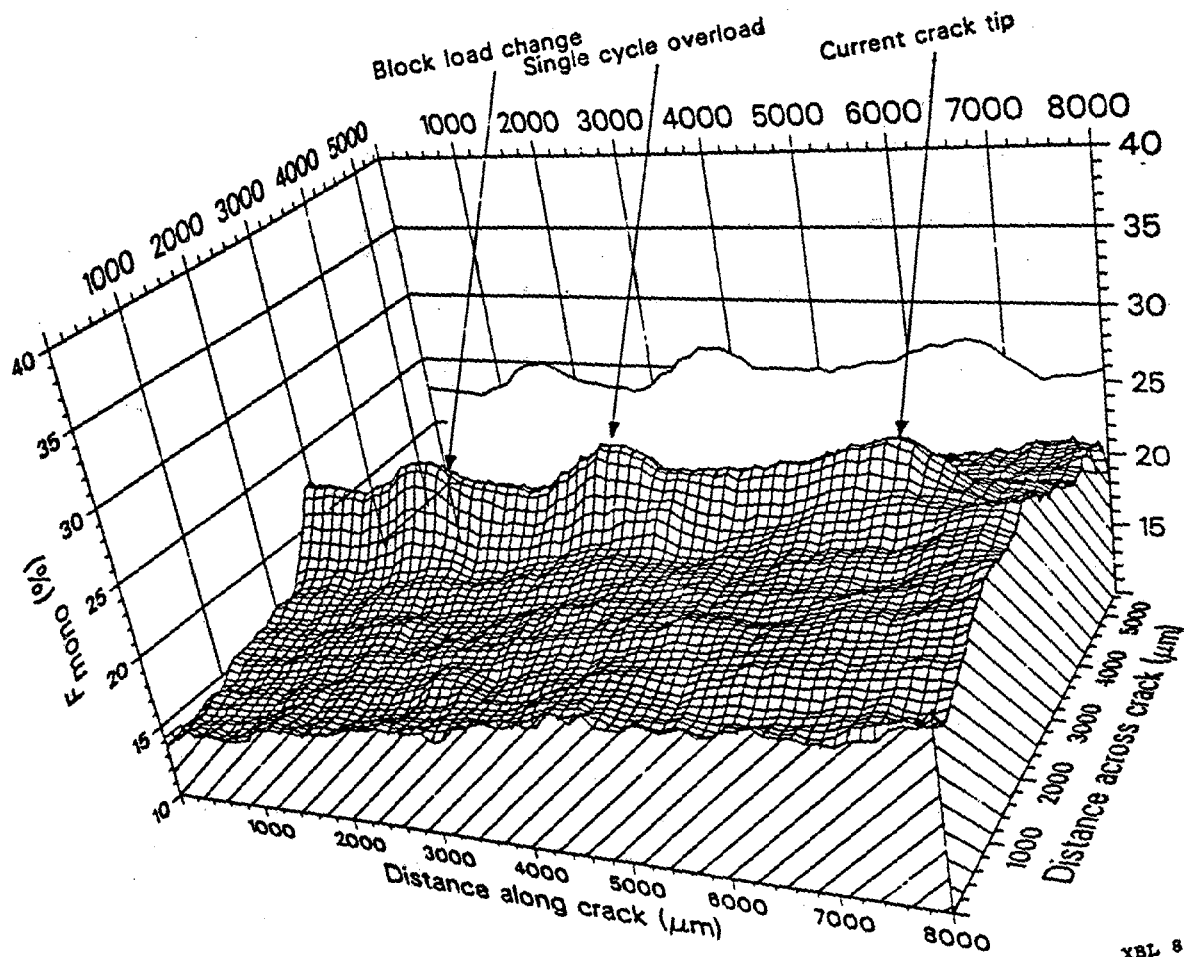Anneal T = 2400 °C

Raman Shift (cm^{-1})

XBL 891-223

21

Fig. 4

XBL 883-6010

Fig. 5

23

Fig. 6

XBL 891-220

24

LAWRENCE BERKELEY LABORATORY
TECHNICAL INFORMATION DEPARTMENT
1 CYCLOTRON ROAD
BERKELEY, CALIFORNIA 94720